Journal of Power Sources 196 (2011) 2971–2978

Contents lists available at ScienceDirect

Journal of Power Sources

journal homepage: www.elsevier.com/locate/jpowsour

Low-temperature sintering and electrical properties of strontium- and magnesium-doped lanthanum gallate with V_2O_5 additive

Sang Bu Ha[a], Yoon Ho Cho[a], Ho-Il Ji[b], Jong-Ho Lee[b], Yun Chan Kang[c], Jong-Heun Lee[a,*]

[a] Department of Materials Science and Engineering, Korea University, Anam-dong, Sungbuk-ku, Seoul 136-713, South Korea
[b] Center for Energy Materials Research, Korea Institute of Science and Technology, Seoul 136-791, South Korea
[c] Department of Chemical Engineering, Konkuk University, Seoul 143-701, South Korea

ARTICLE INFO

Article history:
Received 30 July 2010
Received in revised form 1 November 2010
Accepted 8 November 2010
Available online 24 November 2010

Keywords:
Strontium- and magnesium-doped lanthanum gallate
Solid oxide fuel cell
Vanadium oxide
Sintering additive
Phase purity
Oxide ion conductivity

ABSTRACT

The effects of a V_2O_5 additive on the low-temperature sintering and ionic conductivity of strontium- and magnesium-doped lanthanum gallate (LSGM: $La_{0.8}Sr_{0.2}Ga_{0.8}Mg_{0.2}O_{2.8}$) are studied. The LSGM powders prepared by the glycine nitrate method are mixed with 0.5–2 at.% of $VO_{5/2}$ and then sintered at 1100–1400 °C in air for 4 h. The apparent density and phase purity of the LSGM specimens are increased with increasing sintering temperature and $VO_{5/2}$ concentration due to the enhanced sintering and mass transfer via the intergranular liquid phase. The 1 at.% $VO_{5/2}$-doped LSGM specimen sintered at 1300 °C exhibits a high oxide ion conductivity of ~0.027 S cm^{-1} at 700 °C over a wide range of oxygen partial pressure ($P_{O_2} = 10^{-27} - 1$ atm), thereby demonstrating its potential as a useful electrolyte for anode-supported solid oxide fuel cells (SOFCs) without the requirement for any buffer layer between the electrolyte and anode.

© 2010 Elsevier B.V. All rights reserved.

1. Introduction

Strontium- and magnesium-doped lanthanum gallate (LSGM) is one of the representative electrolytes for application in solid oxide fuel cells (SOFCs) [1,2] on account of its high ionic conductivity and stability over a wide range of oxygen partial pressure ($P_{O_2} = 10^{-22} - 1$ atm). In particular, SOFC operation at low and intermediate temperatures (500–800 °C) facilitates a rapid start-up, operational stability, and the use of cost-effective gas sealing and interconnecting materials. This can be best accomplished by thinning the electrolyte using an anode-supported design [3–6].

The low-temperature densification of the LSGM electrolyte is one of the most important challenges in the fabrication of high-performance LSGM-based SOFCs. At relatively low sintering temperatures, the specimen density is poor and various intermediate phases form due to the complexity in cations [7,8]. Specimen densification up to gas impermeable level can be achieved at a high sintering temperature of ~1500 °C [9]. The interdiffusion of La and Ni components from the Ni-based anode and LSGM electrolyte leads, however, to the formation of a resistive interface phase such as $LaNiO_3$ [10], which deteriorates the SOFC performance. To prevent this, various oxide buffer layers such as lanthanum-doped ceria (LDC), gadolinia-doped ceria (GDC) and scandia-stabilized zirconia (ScSZ) have been employed [11–13].

Until now, the sintering temperature has been decreased either by employing innovative consolidation techniques [14–19] or by preparing easily sinterable powders [20–26]. The design of sintering aids to promote densification can be a practical alternative. In a previous report [27], 1 at.% of 14 different oxide additives was added to LSGM and their effects on the sintering behaviour was examined. The addition of V, Zn, Si, Co, and Fe improved the densification and a.c. electrical conductivity at 300 °C, with V showing the most promising effect. Thus far, the possibility of enhancing the ionic conductivity of LSGM has been explored by the doping of various transition metal oxides [28–35]. The addition of Fe or Co is known to increase ionic conductivity but to decrease the transport number. The effect of V doping on the ionic conductivity of LSGM has not been studied. Accordingly, in order to examine the possibility of V-doped LSGM as a new electrolyte of LSGM-based SOFCs, it is necessary to investigate the electrical conductivity at the operation temperature of SOFCs and its dependence on the oxygen partial pressure (P_{O_2}). Moreover, it is essential to elucidate the role of a V component in grain-interior and grain-boundary conduction, the mechanism of enhanced sintering, and the optimum doping concentration of V.

In this study, the roles of V_2O_5 additive on the densification, phase purity and ionic conductivity of LSGM are systematically investigated by varying the $VO_{5/2}$ concentration and sintering tem-

* Corresponding author. Tel.: +82 2 3290 3282; fax: +82 2 928 3584.
E-mail addresses: jongheun@korea.ac.kr, leejongheun@gmail.com (J.-H. Lee).

0378-7753/$ – see front matter © 2010 Elsevier B.V. All rights reserved.
doi:10.1016/j.jpowsour.2010.11.082

perature. For this, undoped, 0.5, 1 and 2 at.% $VO_{5/2}$-doped LSGM specimens are prepared and investigations are made of the grain-interior and grain-boundary conduction by means of complex impedance spectroscopy, the location of V component using transmission electron microscopy (TEM) and energy dispersive X-ray spectroscopy (EDS), the temperature and P_{O_2} dependence of electrical conductivity, the density and the phase purity. The study focuses on an examination of the V-doped LSGM electrolyte for application in low- and intermediate-temperature SOFCs.

2. Experimental

LSGM ($La_{0.8}Sr_{0.2}Ga_{0.8}Mg_{0.2}O_{2.8}$) powders were prepared by the glycine nitrate method. $La(NO_3)_3{\cdot}6H_2O$ (99.99%, Aldrich, USA), $Sr(NO_3)_2$ (>99%, Sigma–Aldrich, St. Louis, MO, USA), $Ga(NO_3)_3{\cdot}xH_2O$ (99.9%, Aldrich, USA) and $Mg(NO_3)_2{\cdot}6H_2O$ (99%, Sigma–Aldrich, USA) were dissolved in 150 mL of distilled water ($[La^{3+}]:[Sr^{2+}]:[Ga^{3+}]:[Mg^{2+}] = 8:2:8:2$), to which H_2NCH_2COOH (glycine, >99%, Sigma, USA) was added ($[\text{glycine}]/([La^{3+}]+[Sr^{2+}]+[Ga^{3+}]+[Mg^{2+}]) = 1.0$). The polymeric gel precursor was prepared by heating the stock solution at 80 °C for 10 h. The LSGM powders were prepared by calcining the precursors at 1000 °C for 2 h. The particle sizes of the calcined LSGM powders ranged from 30 to 200 nm and the average particle size determined from TEM micrographs was 99.1 ± 54.2 nm. V_2O_5 was added to LSGM powders at 0.5–2 at.% by ball milling a mixture of LSGM and V_2O_5 (99%, Junsei Chemical Co., Tokyo, Japan) powders in C_2H_5OH for 24 h. After drying and pulverization, the specimens were isostatically pressed at 150 MPa and sintered in air at 1100–1400 °C for 4 h. For simplicity, the specimens doped with $[VO_{5/2}] = x$ at.% will be referred as 'LSGM-*x*V-ST' where 'ST' is the sintering temperature. For example, LSGM-0.5V-1250 indicates the 0.5 at.% $VO_{5/2}$-doped LSGM specimen sintered at 1250 °C.

The apparent density of the sintered body was measured using the Archimedes method in deionized water. The crystal phases of the sintered specimens were analyzed by X-ray diffraction (XRD; D/MAX-2500V/PC, Rigaku Co., Tokyo, Japan), and their microstructures were observed by field emission-scanning electron microscopy (FE-SEM; Hitachi S-4300, Hitachi Science Systems Ltd., Hitachi City, Japan) and high resolution-TEM (HR-TEM; Tecnai 20, Philips, Eindhoven, Netherlands). For TEM observations, the sintered specimens were cut, polished, dimpled, and finally ion milled. After applying a Pt electrode using Pt paste (TR7905, Tanaka Co., Tokyo, Japan), the a.c. 2-probe conductivity was measured at 300–700 °C in air using an impedance analyzer (Alpha-N, Novocontrol Tech., Hundsangen, Germany).

The d.c. 4-probe conductivity of the sintered specimen was also measured at a fixed temperature of 700 °C while changing the P_{O_2}. The ambient P_{O_2} was controlled by N_2/O_2 mixtures and $H_2/H_2O/Ar$ mixtures and monitored by YSZ-based oxygen sensors. The P_{O_2} range of examination was $-27 \leq \log P_{O_2} \leq 0$.

3. Results and discussion

3.1. Densification and microstructure

The apparent densities of the undoped LSGM specimens increase as the sintering temperature is increased to 1300 °C and then tend to saturate above 1300 °C (Fig. 1). By contrast, the saturated density could be attained at 1250 °C for the LSGM-1V specimen. The V-induced promotion of sintering is more substantial and reproducible at temperatures ≤1250 °C. The microstructures of the specimens sintered at 1200 and 1300 °C are shown in Fig. 2. When sintered at 1200 °C, many pores are found in the undoped specimen (Fig. 2(a)), while all the V-doped specimens show dense microstructures (Fig. 2(b)–(d)). Grain growth is observed as the sintering temperature is increased to 1300 °C. At 1300 °C, all the specimens, regardless of V doping, have relatively dense microstructures (Fig. 2(e)–(h)). The variation of density as a function of $VO_{5/2}$ concentration and sintering temperature are presented in Fig. 3. The density increases greatly with increasing $VO_{5/2}$ doping concentration and the promotion effect is higher at 1200 and 1250 °C. This demonstrates that the sintering temperature of LSGM for the application of SOFCs can be lowered to 1250 °C by doping with 0.5–2 at.% of $VO_{5/2}$.

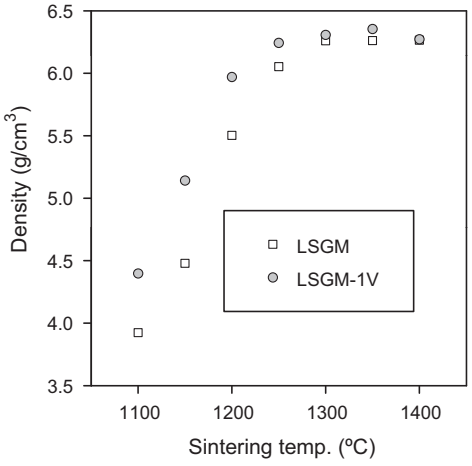

Fig. 1. Apparent densities of undoped and 1 at.% $VO_{5/2}$-doped LSGM specimens with varying sintering temperature.

3.2. Phase purity

The LSGM powders after the calcination of the precursors at 1000 °C contain second phases such as $LaSrGa_3O_7$ (LSG3) and $LaSrGaO_4$ (LSG) (not shown). The amount of LSG3 and LSG phases decreases with increasing sintering temperature (Fig. 4(a), (d) and (g)). The phase purity increases with increasing $VO_{5/2}$ doping concentration (see, for example, Fig. 4(a)–(c)). The PP factor is used as a measure of the LSGM phase purity and is defined as the intensity of peaks for LSG3 and LSG phases relative to that for the LSGM phase, namely:

$$PP = 1 - \frac{I_{\text{LSG3}(211)} + I_{\text{LSG}(103)}}{2I_{\text{LSGM}(112)}} \quad (1)$$

where $I_{\text{LSG3}(211)}$, $I_{\text{LSG}(103)}$ and $I_{\text{LSGM}(112)}$ are the intensities of the (2 1 1) peak of $LaSrGa_3O_7$, the (1 0 3) peak of $LaSrGaO_4$ and the (1 1 2) peak of LSGM, respectively. The *PP* factor is higher for purer LSGM specimens and becomes unity for the completely phase-pure one. At all sintering temperatures (1200–1350 °C), the *PP* factors are increased with increasing $[VO_{5/2}]$ (Fig. 5), which indicates that the increased phase purity is achieved by V doping. In particular, the *PP* factor is increased from 0.89 to 0.96 by the addition of 2 at.% of $VO_{5/2}$ at the sintering temperature of 1300 °C and thereby indicates that an almost phase-pure LSGM specimen can be prepared even at a sintering temperature as low as 1300 °C.

3.3. Temperature dependence of electrical conductivity

The electrical conductivity determined by the a.c. 2-probe method at 300–700 °C is shown in Fig. 6. The electrical conductivity of the LSGM-1V-1300 specimen is higher than that of the LSGM-1300 specimen. The apparent activation energy for conduction (ΔE_{app}) is calculated from the slope of the linear plot between $\ln(\sigma T)$ and $1/T$. The ΔE_{app} value of LSGM-1V-1300 is 1.02 ± 0.01 eV, which is slightly smaller than that of LSGM-1300 (1.05 ± 0.01 eV).

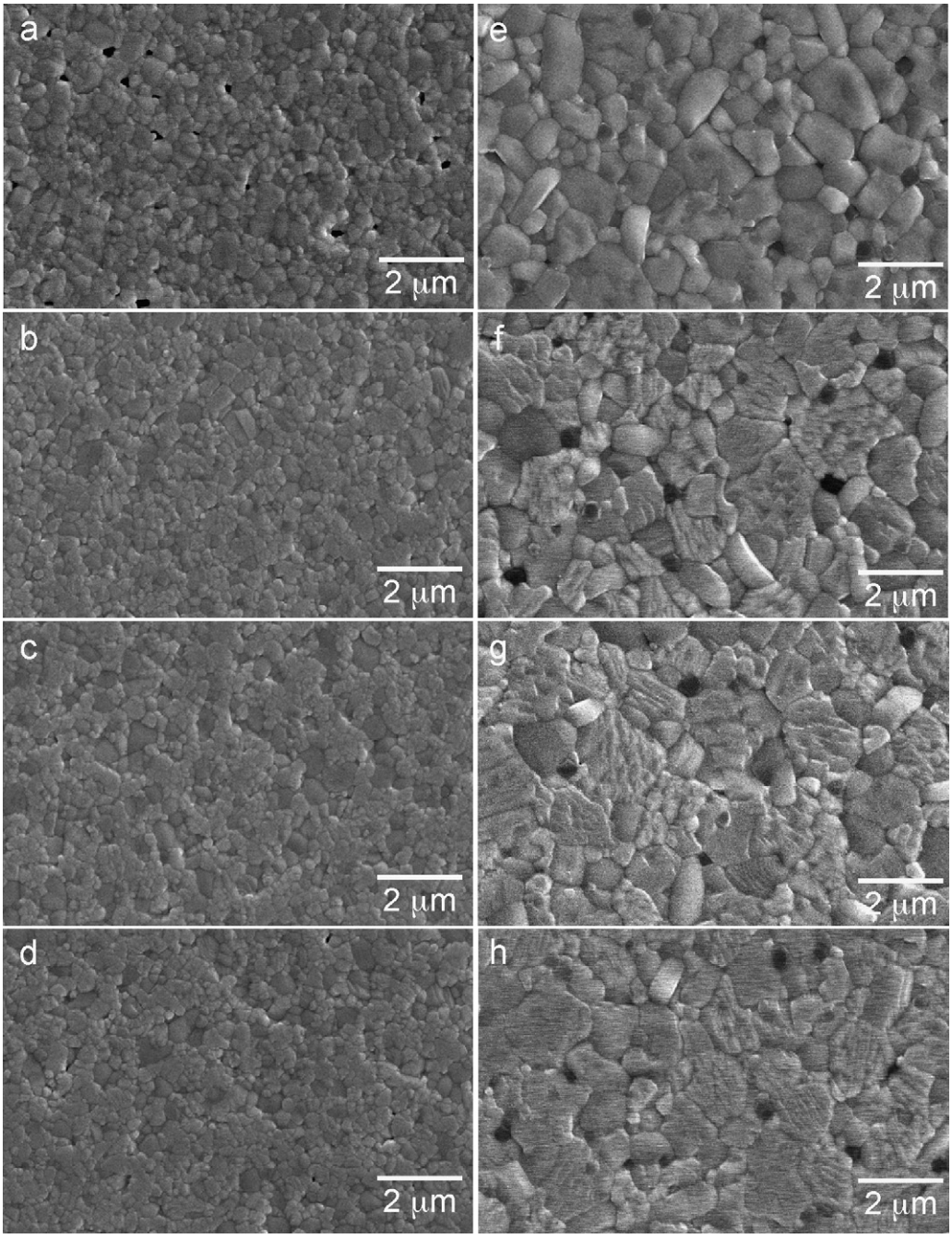

Fig. 2. SEM images of (a) LSGM-1200, (b) LSGM-0.5V-1200, (c) LSGM-1V-1200, (d) LSGM-2V-1200, (e) LSGM-1300, (f) LSGM-0.5V-1300, (g) LSGM-1V-1300, and (h) LSGM-2V-1300.

3.4. Complex impedance analysis and discussion

The effect of V doping in increasing the electrical conductivity and decreasing the ΔE_{app} value is related to various factors such as the incorporation of V into the LSGM lattice, the specimen density (porosity), the composition of the LSGM electrolyte, the existence of a second phase, and the physico-chemical properties of the grain boundary. To aid understanding, the separation of the grain-interior and the grain-boundary contributions from complex impedance spectra can be considered as a useful tool. At high temperatures (500–700 °C), the deconvolution of grain-interior and grain-boundary contributions is difficult because the inductive component from the lead wire becomes relatively dominant against the RC parallel contributions from the bulk and grain boundary. Thus, the grain-interior and grain-boundary resistivity cannot be attained over the entire temperature regime and the apparent activation energies for conduction in the grain interior and across the grain boundary cannot be analyzed. By contrast, well-defined semicircles can be attained in the complex impedance spectra at low temperatures (300–450 °C). Accordingly, the complex impedance at 300 °C is analyzed to investigate the change of grain-interior and grain-boundary resistivity in relation to V doping (Fig. 7). The three contributions from the low-frequency range are those from electrode polarization, grain boundary, and grain interior. The grain-interior resistivity (ρ_{gi}) and apparent grain-boundary resistivity ($\rho_{gb}{}^{app}$) are attained from the impedance spectra and the results are shown in Fig. 8(a) and (b).

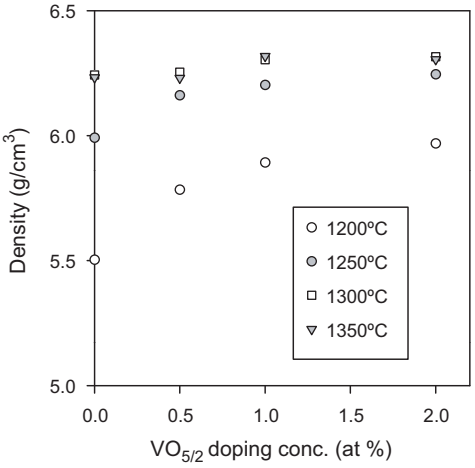

Fig. 3. Apparent densities of LSGM with varying $VO_{5/2}$ concentration and sintering temperature.

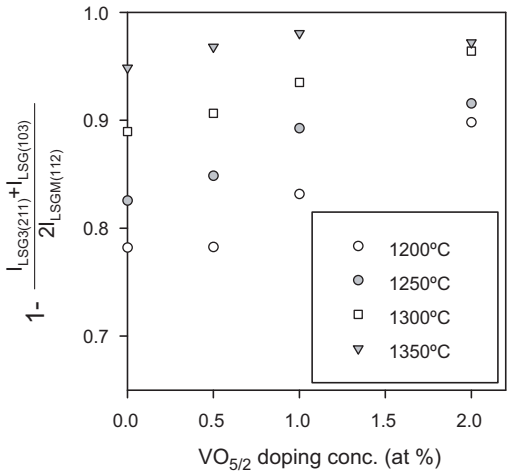

Fig. 5. Phase purity of LSGM with varying $VO_{5/2}$ concentration and sintering temperature. $I_{LSG3(211)}$, $I_{LSG(103)}$, and $I_{LSGM(112)}$ are intensities of (2 1 1) peak of $LaSrGa_3O_7$, (1 0 3) peak of $LaSrGaO_4$, and (1 1 2) peak of LSGM, respectively.

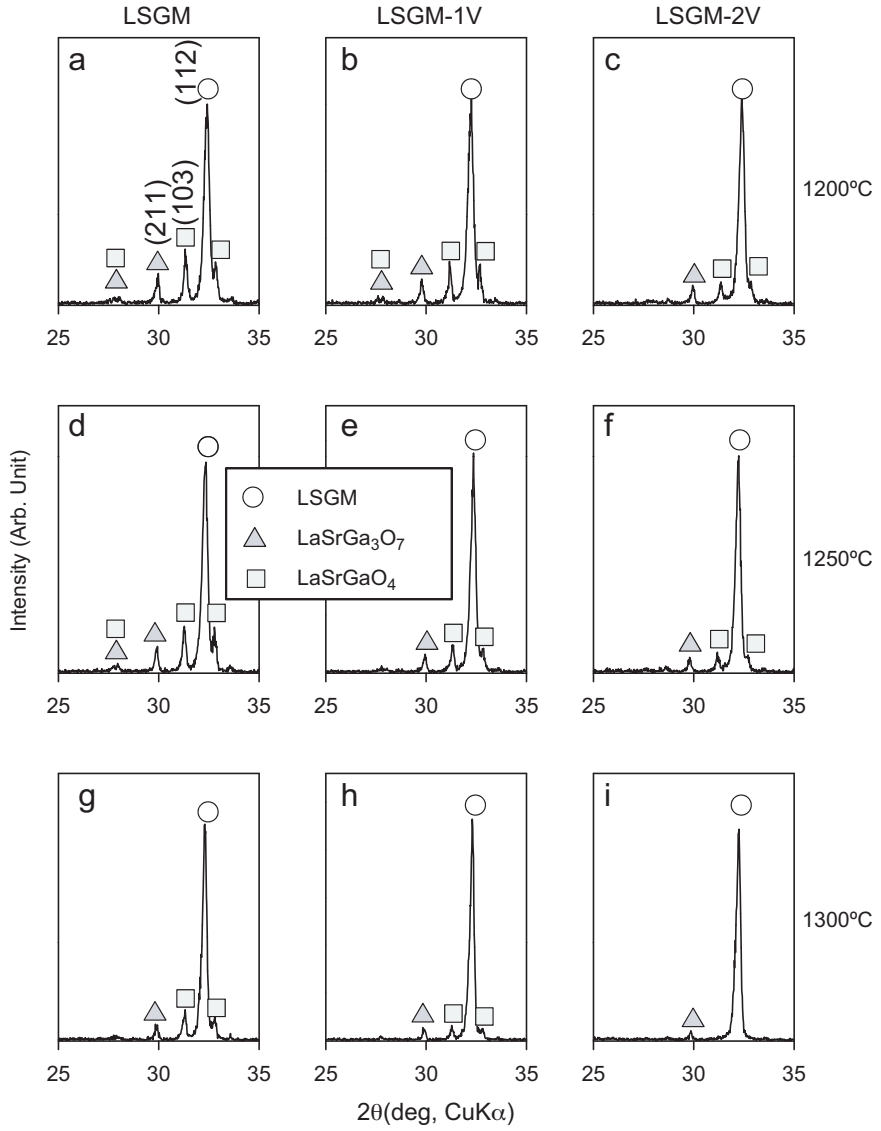

Fig. 4. X-ray diffraction (XRD) patterns of (a) LSGM-1200, (b) LSGM-1V-1200, (c) LSGM-2V-1200, (d) LSGM-1250, (e) LSGM-1V-1250, (f) LSGM-2V-1250, (g) LSGM-1300, (h) LSGM-1V-1300, and (i) LSGM-2V-1300.

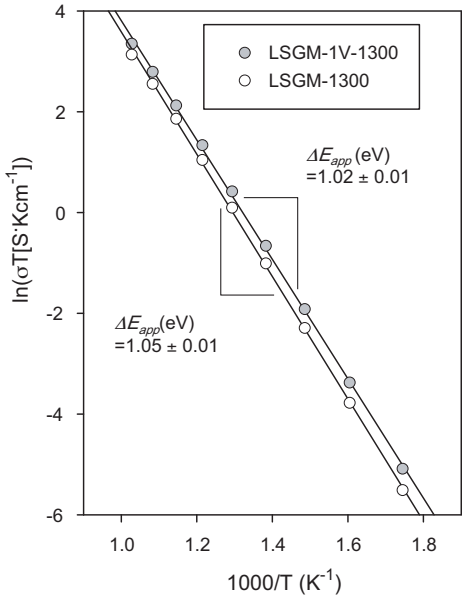

Fig. 6. $\ln \sigma T$ as a function of $1000/T$ and apparent activation energies for conduction (ΔE_{app}) for LSGM-1300 and LSGM-1V-1300.

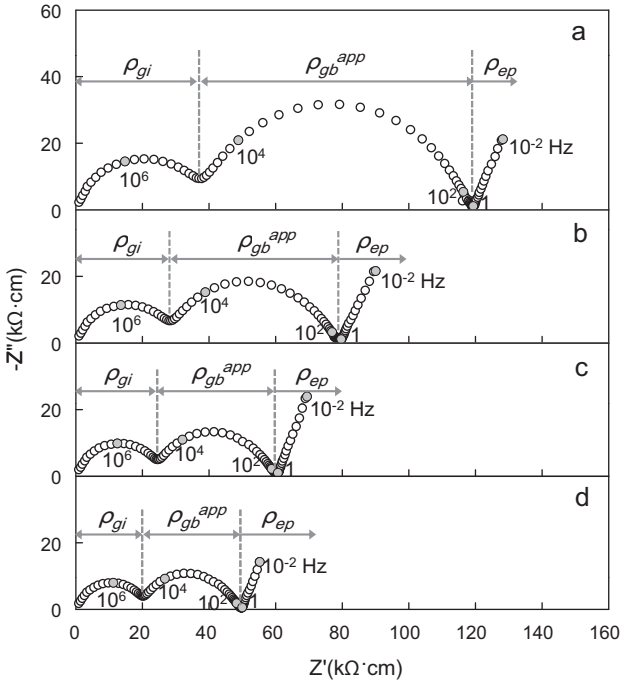

Fig. 7. Complex impedance spectra of (a) LSGM-1300, (b) LSGM-0.5V-1300, (c) LSGM-1V-1300, and (d) LSGM-2V-1300 at 300 °C in air.

At a constant $VO_{5/2}$ doping concentration, the ρ_{gi} values decrease with increasing sintering temperature. As shown in Figs. 3 and 5, the density and phase purity are increased with increasing sintering temperature. The ρ_{gi} value is determined by the apparent electrode area and specimen thickness. Thus, the increase of effective cross-sectional area for conduction by densification can increase the ρ_{gi} value. A uniform and precise electrolyte composition with minimal presence of a resistive second phase in a highly phase-pure specimen would also improve the electrical conductivity. Accordingly, the enhanced grain-interior conductivity at high sintering temperature can be attributed to the high density and phase purity of the specimen with minimal second phase.

At constant sintering temperature, the ρ_{gi} values decrease with increasing $VO_{5/2}$ doping concentration. The ionic radii of La^{3+} and Sr^{2+}, A-site cations in the perovskite structure, at the coordination numbers of 12 are 1.500 and 1.580 Å, respectively [36], whereas those of B-site cations, Ga^{3+} and Mg^{2+}, at the coordination numbers of 6 are 0.760 and 0.860 Å, respectively. The ionic radius of V^{5+} at the coordination number is 0.680 Å, which is significantly smaller than both of the A-site and B-site cations. A consideration of the ionic size suggests that most of the V is not incorporated into the lattice. Even if it were incorporated into the B site, the higher valence of V would not generate more oxygen vacancies. In order to confirm whether V is incorporated into the LSGM lattice or not, the lattice parameter can be measured. The variation of lattice parameters with increasing $VO_{5/2}$ doping concentration cannot, however, be used as an indication of V incorporation because the LSGM composition and the amount of second phases are also dependent upon the $VO_{5/2}$ doping concentration in this study.

The melting point of V_2O_5 is 690 °C [37,38]. V_2O_5 is known to form an intergranular liquid phase at relatively low temperature and to promote densification via liquid phase sintering [37–40]. This is consistent with the present results, namely, that the density and phase purity are increased by increasing $VO_{5/2}$ doping concentration (Figs. 3 and 5). Thus, in the present study, most of the V is not incorporated into the LSGM lattice but acts as the precursor of the intergranular liquid phase to promote sintering and mass transfer. When sintered at 1200 and 1250 °C, the density and phase purity are increased significantly by the addition of V_2O_5 (Figs. 3 and 5), both of which decrease the ρ_{gi} values. In the specimens sintered at 1300 °C, the decrease of ρ_{gi} is dominated by the increase of phase purity (Figs. 3 and 5). Finally, although the enhancement is not large, the density and phase purity are slightly increased with V doping at the sintering temperature of 1350 °C, which can explain the enhancement of grain-interior conduction. Therefore, in overall, the V doping-induced decrease in the ρ_{gi} values (Fig. 8(a)) can be explained by the increased phase purity and density.

The $\rho_{gb}{}^{app}$ values are also decreased with increasing sintering temperature and $VO_{5/2}$ doping concentration although the values fluctuated slightly in LSGM-1V-1350 and LSGM-2V-1350 (Fig. 8(b)). The $\rho_{gb}{}^{app}$ values are calculated from the cross-sectional area (A) and thickness (l) of the specimen. Precise measurement of the thickness of the resistive grain-boundary phases (δ_{gb}) for specific analysis is hampered, however, by the distribution of the space charge layer, the grain-boundary structures, and the configuration of the intergranular phase. Nevertheless, an approximate specific grain-boundary resistivity ($\rho_{gb}{}^{sp}$) can be calculated from the ratio of the capacitances of the grain interior and grain boundary using the following assumptions [41]: (i) a brick layer model, (ii) $\rho_{gb}{}^{sp} \gg \rho_{gi}$, (iii) grain size ($d_g$) $\gg \delta_{gb}$, and (iv) the permittivity of the grain-boundary phase (ε_{gb}) ≅ the permittivity of the grain-interior phase (ε_{gi})

$$\rho_{gb}^{sp} = \frac{C_2}{C_1}\rho_{gb}^{app} \quad (2)$$

where C_1 and C_2 are the capacitances of the grain-interior and grain-boundary components obtained by deconvolution of the impedance spectra.

The results are shown in Fig. 8(c). With a range of 4450–8680 kΩ cm (Fig. 8(c)), the $\rho_{gb}{}^{sp}$ values are 105.0–283.8 times larger than the ρ_{gi} values. This indicates that the grain boundary of the undoped and V-doped LSGM specimens is a few hundred times more resistive than the grain interior. The $\rho_{gb}{}^{sp}$ values of LSGM-1V and LSGM-2V are similar, regardless of the sintering temperature, whereas those of LSGM and LSGM-0.5V are increased by ~50% as the sintering temperature is increased from 1200 to 1350 °C. By contrast, at constant composition, the $\rho_{gb}{}^{app}$ values of the specimens varies 10.8–26.2 times with the variation of sintering

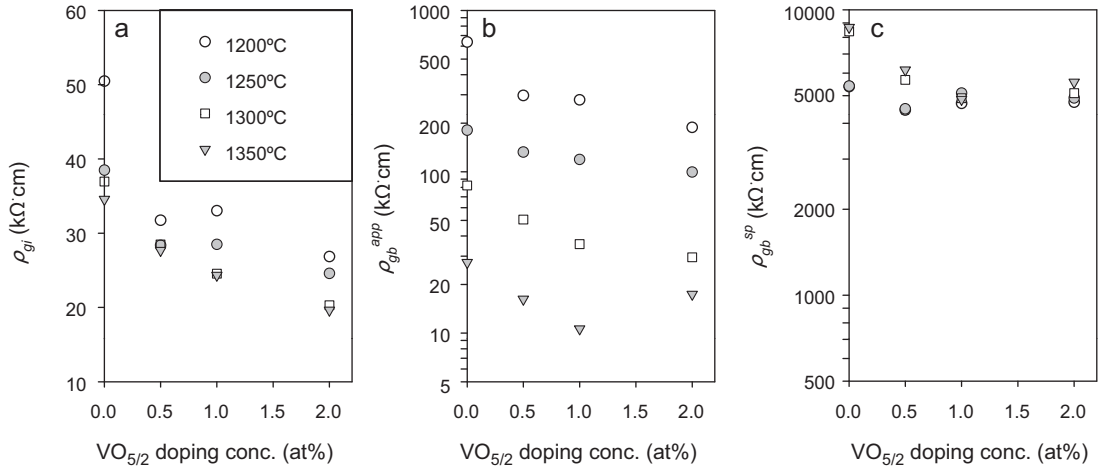

Fig. 8. (a) Grain-interior resistivity (ρ_{gi}), (b) apparent grain-boundary resistivity ($\rho_{gb}{}^{app}$) and (c) specific grain-boundary resistivity ($\rho_{gb}{}^{sp}$) of LSGM with varying $VO_{5/2}$ concentration and sintering temperature.

temperature (Fig. 8(b)). This suggests that the significant decrease of $\rho_{gb}{}^{app}$ with increasing sintering temperature (Fig. 8(b)) is mainly due to the decreased grain-boundary density by grain growth.

The average grain sizes of LSGM-1300, LSGM-0.5V-1300, LSGM-1V-1300 and LSGM-2V-1300 were 1.18, 1.44, 1.46 and 1.62 μm, respectively, as calculated from about 400 grains. This indicates that the V-induced decrease of $\rho_{gb}{}^{app}$ values is partly due to the grain coarsening. At the sintering temperatures of 1200 and 1250 °C, the $\rho_{gb}{}^{sp}$ values remain similar regardless of the $VO_{5/2}$ doping concentration (Fig. 8(c)). By contrast, when sintered at 1300 and 1350 °C, the $\rho_{gb}{}^{sp}$ values decreases with increasing $VO_{5/2}$ doping concentration (Fig. 8(c)). It has not been possible to elucidate why the grain boundary becomes more conductive with V_2O_5 addition when sintered at 1300 and 1350 °C and further study is required. Nevertheless, the grain-boundary conduction is not affected by the addition of V_2O_5.

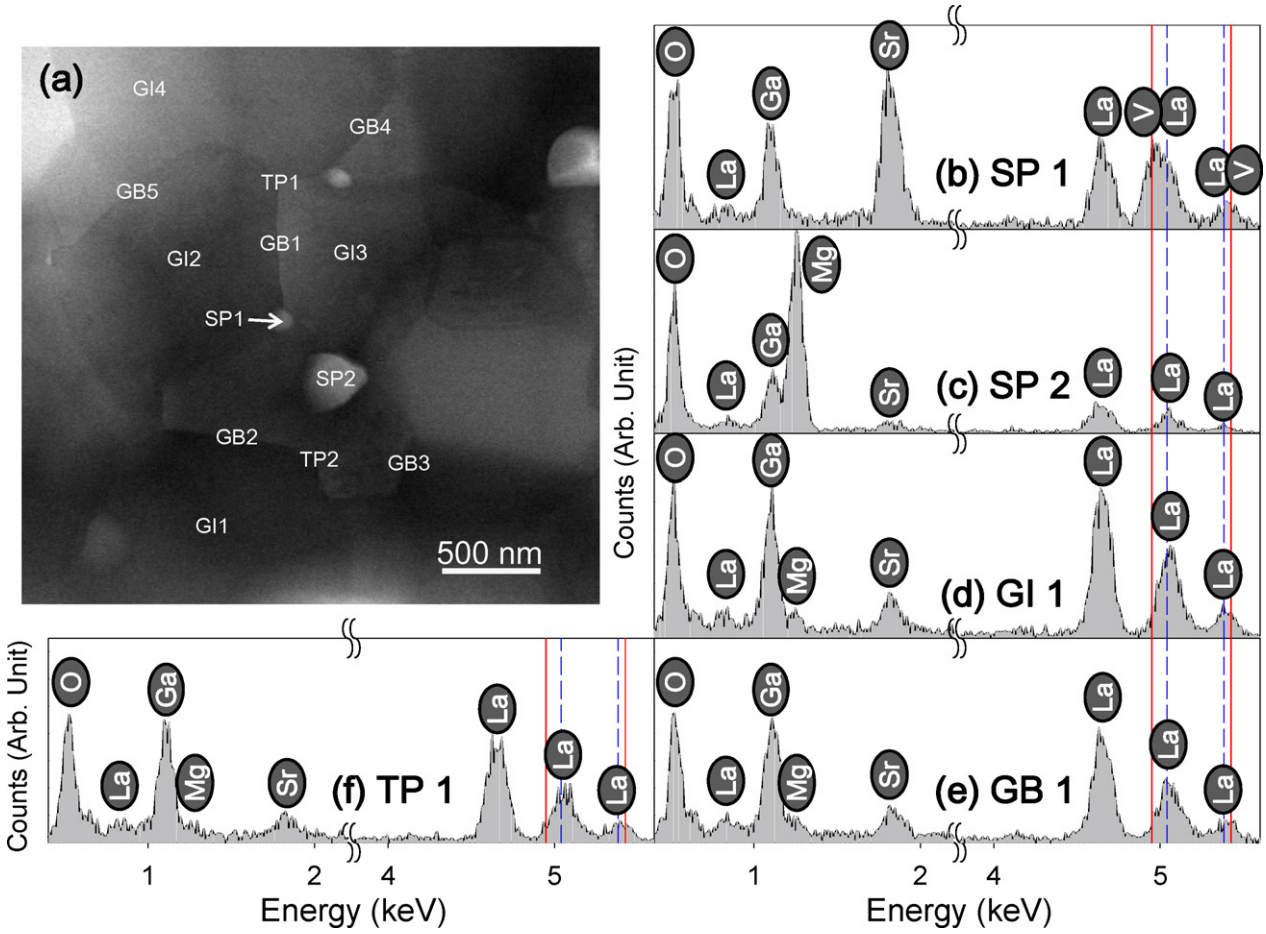

Fig. 9. (a) Transmission electron micrograph of LSGM-1V-1300 and EDS results at (b) and (c) second phase (denoted as SP), (d) grain-interior (denoted as GI), (e) grain boundary (denoted as GB), and (f) triple joint (denoted as TP).

3.5. TEM analysis

In solid electrolytes doped with acceptors such as zirconia and ceria, it is known that the siliceous intergranular liquid phase virtually blocks grain-boundary conduction [42–49], although it can promote densification via a liquid phase sintering mechanism [50]. In the present study, considering the amorphous configuration, the intergranular liquid phase containing V_2O_5 may have also played a deleterious role in the grain-boundary conduction. Nevertheless, the grain-boundary conduction is not affected by V_2O_5 addition. To determine the reason, the location of V was investigated using TEM and EDS (Fig. 9). V is not detected at the grain interior (GI1, GI2, GI3, GI4 in Fig. 9(a) and (d)), which further reduces the plausibility of V incorporation into the LSGM lattice. Nor is any significant V component observed at most of the grain boundaries (GB1, GB2, GB3, GB4, GB5 in Fig. 9(a) and (e)) or in the triple junctions between the grain boundaries (TP1, TP2 in Fig. 9(a) and (f)). Among the Sr- and Mg-rich second phases (SP1 and SP2 in Fig. 9(a)) located at the triple junctions, most of the V component is found at the former (SP1 in Fig. 9(a) and (b)). These tendencies are further confirmed by repetitive analysis on other Sr-rich second phases. These relatively clean grain boundaries indicate that the intergranular phase containing V after liquid phase sintering is gathered around the Sr-rich second phase.

Previously, it was reported [51] that the grain-boundary conduction of LSGM is barely affected by the addition of even 2000 ppm SiO_2 to LSGM, while that of GDC is significantly deteriorated. The siliceous phase is scavenged near the Sr-rich phase rather than the Mg-rich one, which is attributed to the higher chemical affinity between SrO and the acidic siliceous intergranular phase as a result of the greater basicity, according to cationic field strength, of SrO compared with MgO [52]. The cationic field strength of V_2O_5 is similar to that of SiO_2 (1.57) [53] and thereby indicates that V_2O_5 is acidic. Thus, after V_2O_5-assisted liquid phase sintering, most of the intergranular phase containing V is gathered near the more basic Sr-rich second phase along the grain boundary. This explains the relatively clean and conductive grain boundary even after V doping.

3.6. P_{O_2} dependence of electrical conductivity

In order to elucidate the effects of V doping on the LSGM oxide ion conductivity, the electrical conductivities of four sintered samples were measured as a function of P_{O_2} by a conventional d.c. 4-probe method at 700 °C (Fig. 10). For comparison, the LSGM-CON-1470 sample was prepared by sintering commercial LSGM powder (Seimi Chemical, Chigasaki City, Japan) at 1470 °C for 3 h. All the specimens exhibit approximately constant conductivity over a wide range of P_{O_2} from $P_{O_2} = 10^{-27} - 1$ atm, which suggests that ionic conduction in the P_{O_2} regime is not affected by V doping. The approximately constant conductivity, regardless of P_{O_2}, is a further indication that most of the V is not incorporated into the LSGM lattice.

The electrical conductivity of LSGM-1V-1300 (~0.027 S cm^{-1}) is higher than that of LSGM-1300 (~0.022 S cm^{-1}), probably because of the aforementioned V doping effect. The electrical conductivities of LSGM-1300 and LSGM-1V-1300, however, are still smaller than those of single-phase LSGM-1400 (~0.085 S cm^{-1}) and LSGM-CON-1470 (~0.072 S cm^{-1}). The *PP* factors of LSGM-1400 and LSGM-CON-1470 are ~1 while those of LSGM-1300 and LSGM-1V-1300 are 0.890 and 0.935, respectively. By contrast, the increase of density by the elevation of sintering temperature to 1400 and 1470 °C is small. Thus the higher conductivity of LSGM-1400 and LSGM-CON-1470 is mainly due to the enhanced phase purity. Nevertheless, the LSGM-1V-1300 specimen in the present study can be advantageous in the anode-supported design of a SOFC. The typical thickness of the electrolyte in anode-supported SOFCs (~20 μm) is approximately one-tenth of that in electrolyte-supported SOFCs (~200 μm). Accordingly, consideration of both the ionic conductivity and the thickness suggests that the conductance of the LSGM-1V-1300 electrolyte in the anode-supported design can be 3.2–3.8 times higher than that of dense LSGM-1400 or LSGM-CON-1470 electrolytes in the electrolyte-supported design. The resistive interface phase between the LSGM electrolyte and the Ni-based anode forms by interdiffusion of La and Ni components at ≥1350 °C during sintering [54,55]. This indicates that sintering of the electrolyte at ≤1300 °C will minimize the detrimental interface reaction and thus remove the oxide buffer layer between the electrolyte and anode. Accordingly, the LSGM electrolyte with a V_2O_5 additive can provide a high ionic conductivity, anode-supported SOFC design without oxide buffer layer, and good stability over a wide range of P_{O_2} (10^{-27}–1 atm).

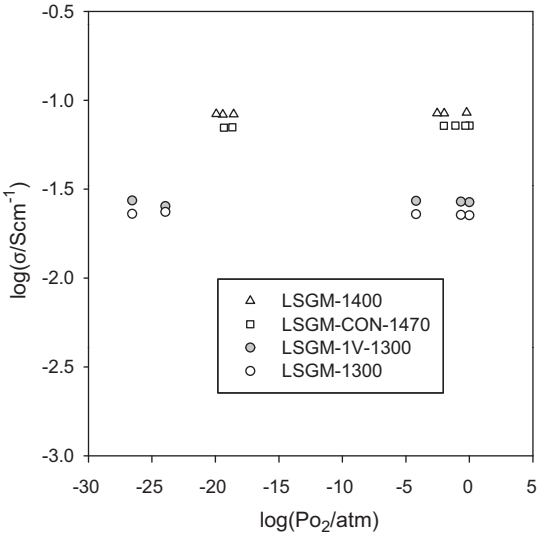

Fig. 10. Electrical conductivity of LSGM ($La_{0.8}Sr_{0.2}Ga_{0.8}Mg_{0.2}O_{2.8}$) as function of oxygen partial pressure (P_{O_2}).

4. Conclusion

The effects of V_2O_5 additive on the densification, crystal phase, and electrical conductivity of LSGM have been investigated. The addition of V_2O_5 promotes the densification and increases the phase purity, which are attributed to enhanced sintering and mass transfer via V_2O_5-assisted liquid phase sintering. At a sintering temperature of 1300 °C, the electrical conductivity of LSGM is increased by the addition of 1 at.% of $VO_{5/2}$. The results from TEM and EDS analyses suggest that most of the V is not incorporated into the LSGM lattice but acts as a precursor for the intergranular liquid phase. The effect of V_2O_5 addition on the grain-interior and grain-boundary conduction is analyzed and discussed using complex impedance analysis. The LSGM-1V-1300 specimen shows a high ionic conductivity (~0.027 S cm^{-1}) over a wide P_{O_2} range ($P_{O_2} = 10^{-27} - 1$ atm). This suggests that the addition of V_2O_5 to a LSGM electrolyte is advantageous for the fabrication of anode-supported SOFCs using an LSGM electrolyte at a low sintering temperature (≤1300 °C) without oxide buffer layer.

Acknowledgements

This work was supported by the Korea Science and Engineering Foundation (KOSEF) NRL program grant funded by the Korean Government (MEST) (no. R0A-2008-000-20032-0) and by the New

& Renewable Energy R&D program (20093020030040) under the Korea Ministry of Knowledge Economy (MKE).

References

[1] T. Ishihara, J. Am. Chem. Soc. 116 (1994) 3801–3803.
[2] M. Feng, J.B. Goodenough, Eur. J. Solid State Inorg. Chem. T31 (1994) 663–672.
[3] W. Guo, J. Liu, Y. Zhang, Electrochim. Acta 53 (2008) 4420–4427.
[4] F. Bozza, R. Polini, E. Traversa, Electrochem. Commun. 11 (2009) 1680–1683.
[5] C.–H. Lo, C.–H. Tsai, C. Hwang, Int. J. Appl. Ceram. Technol. 6 (2009) 513–524.
[6] T. He, Q. He, L. Pei, Y. Ji, J. Liu, J. Am. Ceram. Soc. 89 (2006) 2664–2667.
[7] P. Datta, P. Majewski, F. Aldinger, Mater. Chem. Phys. 102 (2007) 240–244.
[8] R. Polini, A. Pamio, E. Traversa, J. Eur. Ceram. Soc. 24 (2004) 1365–1370.
[9] P. Majewski, T. Maldener, Int. J. Appl. Ceram. Technol. 6 (2009) 249–256.
[10] P. Huang, A. Horky, A. Petric, J. Am. Ceram. Soc. 82 (1999) 2402–2406.
[11] X. Zhu, K. Suna, S. Lea, N. Zhang, Q. Fu, X. Chen, Electrochim. Acta 54 (2008) 862–867.
[12] K.N. Kim, B.K. Kim, J.W. Son, J. Kim, H.-W. Lee, J.-H. Lee, J. Moon, Solid State Ionics 177 (2006) 2155–2158.
[13] K. Huang, R.S. Tichy, J.B. Goodenough, C. Milliken, J. Am. Ceram. Soc. 81 (1998) 2581–2585.
[14] B. Liu, Y. Zhang, J. Alloys Compd. 458 (2008) 383–389.
[15] F. Maglia, U. Anselmi-Tamburini, G. Chiodelli, H.E. Çamurlu, M. Dapiaggi, Z.A. Munir, Solid State Ionics 180 (2009) 36–40.
[16] J. Chang, H.-W. Lee, S.-J.L. Kang, J. Am. Ceram. Soc. 92 (2009) 927–930.
[17] S.V. Kesapragada, S.B. Bhaduri, S. Bhaduri, P. Singh, J. Power Sources 124 (2003) 499–504.
[18] R. Subasri, T. Mathews, O.M. Sreedharan, Mater. Lett. 57 (2003) 1792–1797.
[19] M. Ohnuki, K. Fujimoto, S. Ito, Solid State Ionics 177 (2006) 1729–1732.
[20] P.-S. Cho, S.-Y. Park, Y.H. Cho, S.-J. Kim, Y.C. Kang, T. Mori, J.-H. Lee, Solid State Ionics 180 (2009) 788–791.
[21] N.S. Chae, K.S. Park, Y.S. Yoon, I.S. Yoo, J.S. Kim, H.H. Yoon, Colloids Surf. A: Physicochem. Eng. Aspects 313–314 (2008) 154–157.
[22] D. Lee, J.-H. Han, Y. Chun, R.-H. Song, D.R. Shin, J. Power Sources 166 (2007) 35–40.
[23] M. Shi, N. Liu, Y. Xu, Y. Yuan, P. Majewski, F. Aldinger, J. Alloys Compd. 425 (2006) 348–352.
[24] D.S. Jung, H.Y. Koo, H.C. Jang, J.H. Kim, Y.H. Cho, J.-H. Lee, Y.C. Kang, J. Alloys Compd. 487 (2009) 693–697.
[25] P. Gonçalves, F.M. Figueiredo, Solid State Ionics 179 (2008) 991–998.
[26] H. Ishikawa, M. Enoki, T. Ishihara, T. Akiyama, J. Alloys Compd. 430 (2007) 246–251.
[27] S.B. Ha, Y.H. Cho, Y.C. Kang, J.-H. Lee, J.-H. Lee, J. Eur. Ceram. Soc. 30 (2010) 2593–2601.
[28] T. Ishihara, T. Akbay, H. Furutani, Y. Takita, Solid State Ionics 113–115 (1998) 585–591.
[29] N. Trofimenko, H. Ullmann, Solid State Ionics 118 (1999) 215–227.
[30] T. Ishihara, H. Furutani, M. Honda, T. Yamada, T. Shibayama, T. Akbay, N. Sakai, H. Yokogawa, Y. Takita, Chem. Mater. 11 (1999) 2081–2088.
[31] N. Trofimenko, H. Ullmann, Solid State Ionics 124 (1999) 263–270.
[32] J.W. Stenvenson, K. Hasinska, N.L. Canfield, T.R. Armstrong, J. Electrochem. Soc. 147 (2000) 3213–3218.
[33] B.A. Khorkounov, H. Näfe, F. Aldinger, J. Solid State Electrochem. 10 (2006) 479–487.
[34] M. Enoki, J. Yan, H. Matsumoto, T. Ishihara, Solid State Ionics 177 (2006) 2053–2057.
[35] T. Ishihara, T. Shibayama, M. Honda, H. Nishiguchi, Y. Takita, J. Electrochem. Soc. 147 (2000) 1332–1337.
[36] R.D. Shannon, Acta Crystallogr. A32 (1976) 751–767.
[37] K.A. Yee, K.R. Han, H.T. Kim, J. Mater. Sci. 34 (1999) 4699–4704.
[38] Z. Yao, H. Liu, Z. Shen, Z. Chen, Z. Wu, H. Yu, M. Cao, Mater. Res. Bull. 41 (2006) 1972–1978.
[39] C.-L. Huang, Y.-B. Chen, C.-F. Tasi, J. Alloys Compd. 454 (2008) 454–459.
[40] Y.-C. Chien, C.-H. Hsu, K.-C. Chen, Ferroelectrics 393 (2009) 54–62.
[41] S.M. Haile, D.L. West, J. Campbell, J. Mater. Res. 13 (1998) 1576–1595.
[42] J.-H. Lee, T. Mori, J.-G. Li, T. Ikegami, M. Komatsu, H. Haneda, J. Electrochem. Soc. 147 (2000) 2822–2829.
[43] R. Gerhardt, A.S. Nowick, J. Am. Ceram. Soc. 69 (1986) 641–646.
[44] T.S. Zhang, J. Ma, Y.J. Leng, S.H. Chan, P. Hing, J.A. Kilner, Solid State Sci. 6 (2004) 565–572.
[45] Y.H. Cho, P.-S. Cho, G. Auchterlonie, D.K. Kim, J.-H. Lee, D.-Y. Kim, H.-M. Park, J. Drennan, Acta Mater. 55 (2007) 4807–4815.
[46] P. Jasinski, V. Petrovsky, T. Suzuki, H.U. Anderson, J. Electrochem. Soc. 152 (2005) J27–J32.
[47] X. Guo, R. Waser, Prog. Mater. Sci. 51 (2006) 151–210.
[48] P.-S. Cho, S.B. Lee, Y.H. Cho, D.-Y. Kim, H.-M. Park, J.-H. Lee, J. Power Sources 183 (2008) 518–523.
[49] S.-Y. Park, P.-S. Cho, S.B. Lee, H.-M. Park, J.-H. Lee, J. Electrochem. Soc. 156 (2009) B891–B896.
[50] J.H. Moon, H.M. Jang, B.D. You, J. Mater. Res. 8 (1993) 3184–3191.
[51] Y.H. Cho, S.-B. Ha, D.S. Jung, Y.C. Kang, J.-H. Lee, Electrochem. Solid State Lett. 13 (2010) B28–B31.
[52] J.-H. Lee, Monatsh Chem. 140 (2009) 1081–1094.
[53] C. Zhang, R. Ye, J. Non-Cryst. Solids 112 (1989) 244–250.
[54] N. Maffei, G. de Silveira, Solid State Ionics 159 (2003) 209–216.
[55] X. Zhang, S. Ohara, R. Maric, K. Mukai, T. Fukai, H. Yoshida, M. Nishimura, T. Inagaki, K. Miura, J. Power Sources 83 (1999) 170–177.